ISSN1027-5495. Functional Materials, 30, No.2 (2023), p. 243-254
doi:http://dx.doi.org/10.15407/fm30.02.243

MHD ternary hybrid nanofluid flow over a porous stretching sheet with various effects of Boussinesq and Rosseland approximations

M.I. Kopp[1], V.V. Yanovsky[1,2]

[1] Institute for Single Crystals, NAS Ukraine,
Nauky Ave. 60, Kharkov 61001, Ukraine
[2] V.N. Karazin Kharkiv National University 4 Svobody Sq.,
Kharkov 61022, Ukraine

Received January 11,2023

In this paper, we study the magnetohydrodynamic (MHD) flow of a ternary hybrid nanofluid in a porous medium caused by a stretching sheet under conditions of heat ab- sorption/generation and the action of thermal radiation. The stationary convective flow of a ternary hybrid nanofluid is considered in the case of linear, quadratic, and nonlinear Rosseland approximations, taking into account Boussinesq quadratic thermal oscillations. Basic partial differential equations (PDEs) are transformed into ordinary differential equa- tions (ODEs) using similarity transformations. There are three types of nanoparticles in the fluid flow: spherical, cylindrical, and platelets. The boundary value problem (*bvp*) is used in the Maple computer software to solve transformed equations numerically. The computed results for relevant parameters such as velocity profile, temperature profile, skin friction coefficient, local Nusselt number are visually shown and explained in detail.

Keywords: magnetohydrodynamic flow, ternary hybrid nanofluid, nonlinear Boussinesq approximation, thermal radiation of Rosseland, stretching sheet.

МГД течія потрійної гібридної нанорідини по пористому листі, що розтягується, з різними ефектами наближень Буссинеска і Росселанда. *М. Й. Копп, В. В. Яновський.*

В цій роботі досліджується МГД течія потрійної гібридної нанорідини в пористому середовищі, викликана розтягуванням листа, в умовах поглинання/виділення тепла та впливу теплового випромінювання. Розглянуто стаціонарну конвективну течію потрійної гібридної нанорідини у лінійному, квадратичному та нелінійному наближеннях Росселанда з урахуванням квадратичних теплових коливань Бусінеска. Основні диференційни рівняння у часткових похідних (РЧП) перетворюються на звичайні диференційни рівняння (ЗДР) за допомогою перетворень подібності. У потоці рідини присутні три типи наночастинок: сферичні, циліндричні та пластинчасті. Крайова задача (*bvp*) використовується у програмному забезпеченні Maple для чисельного розв'язання перетворених рівнянь. Результати обчислень для відповідних параметрів, таких як профіль швидкості, температурний профіль, коефіцієнт поверхневого тертя, локальне число Нуссельта наочно показані і докладно пояснені.

systems, combustion, geothermal energy, reactor safety, electronics cooling, solar collectors, etc., it is necessary to take into account the phenomenon of nonlinearity in changes in temperature and density when working at high temperatures. The effect of free convection becomes important when studying the flow of a fluid caused by a vertically expanding heated sheet if the temperature difference between the sheet and

systems, combustion, geothermal energy, reactor safety, electronics cooling, solar collectors, etc., it is necessary to take into account the phenomenon of nonlinearity in changes in temperature and density when working at high temperatures. The effect of free convection becomes important when studying the flow of a fluid caused by a vertically expanding heated sheet if the temperature difference between the sheet and the surrounding fluid is large enough to cause density gradients in the fluid and due to gravity creating a buoyant force. In this case, the density fluctuations are nonlinear, and therefore the linear Boussinesq approximation is no longer suitable for such applications.

In this regard, Goren [1] obtained an expression for density variations that takes into account the quadratic temperature difference. Vajravelu and Sastri [2] found an expression for the density $\rho(T)$ using the Taylor expansion in surface temperature T_∞, taking into account quadratic temperature fluctuations. They found that the effect of the quadratic Boussinesq approximation has a noticeable effect on the velocity and temperature fields. In a porous non-Darcy medium, Partha [3] shown that the velocity profile increases as the nonlinear convection's parameters are increased. RamReddy [4], using the nonlinear/quadratic Boussinesq approximation, investigated the power-law fluid's natural convective flow over an inclined plate.

With the development of nanotechnology, a new type of liquid has arisen, the so-called nanofluids [5]. A nanofluid is a colloidal suspension of a nanoscale particle in a base fluid. Metals, oxides, carbides, and carbon nanotubes are commonly used as nanoparticles, while water and ethylene glycol are used as the base fluid. Nanofluids have a greater thermal conductivity than regular fluids, which is needed for the efficient transfer of thermal energy. Nanofluids can take the role of current refrigerants in a number of sectors, including energy, electronics, transportation, and manufacturing. In regard to this, since the discovery of this original concept, researchers have been particularly interested in the uses of nanofluids. The suspension of many nanoparticles in the base fluid results in the creation of a novel type of nanofluid known as a hybrid nanofluid.

Another important aspect is the study of the phenomenon of thermal radiation in the heat flow of the boundary layer. The model was developed by Rosseland [6] to study heat radiation for coarse and gray medium, and it has been widely applied. Viskanta and Grosh [7], Perdikis and Raptis [8], and Cortell [9] all used the linearized form of the Rosseland radiative heat flux in their studies of boundary layer heat transfer under the assumption that the system has a small temperature difference.

However, in fluid flow systems where a larger thermal flow is needed, linear radiations are not suitable; instead, nonlinear thermal radiations are used. Pantokratoras [10] investigated the Rosseland radiation without any simplification and took into account the system's large temperature difference. Nevertheless, in [10] considered the linear Boussinesq approximation of the buoyancy force. The effect of nonlinear thermal radiation on fluid flow near a vertical porous plate in the quadratic Boussinesq approximation was considered by Jha and Samaila [11]. Waqas et al. [12] looked into the effect of nonlinear thermal radiation on the non-Newtonian nanofluid flow over a vertical plate subject to convective boundary conditions. Their results demonstrate that the temperature field is enhanced by nonlinear radiation. Recently, Mahanthesh [13] considered quadratic radiation and quadratic Boussinesq approximation on hybrid nanoliquid in the Sakiadis flow of a hybrid nanofluid past a vertical plate. Thriveni and Mahanthesh [14] investigated the effects of quadratic radiation and the quadratic Boussinesq approximation on the transport of hybrid nanofluids and determined that these effects improve the heat transport of the fluid system. Mahanthesh et al. [15] studied the flow of a non-Newtonian nanofluid (Jeffrey nanofluid) driven by a flexible surface subjected to quadratic thermal radiation and the quadratic Boussinesq approximation. They found that the heat transfer rate is more sensitive to quadratic thermal radiation than to the zig-zag movement of nanoparticles and thermophoretic characteristics.

In recent years, a new class of nanofluids has emerged, consisting of three solid nanoparticles distributed in an ordinary liquid. The term ternary hybrid nanofluid is commonly used to describe these liquids [16]. Recent studies [17]-[20] by numerous researchers looked at the thermal properties of ternary fluid.

Guedri et al. [21] studied the two-dimensional nonlinear convective flow of a ternary hybrid nanofluid on a nonlinearly stretching sheet, taking into account the quadratic Boussinesq approximation and nonlinear thermal radiation. They concluded that the hydrodynamic characteristics decrease with increasing

values of the volume fraction of solid nanoparticles, porosity, and inertia coefficients and increase at higher values of the thermal and nonlinear thermal Grashof numbers. The effect of linear and nonlinear Rosseland approximations on the three-dimensional flow behavior of a ternary hybrid nanofluid was studied by Sajjan et al. [22] in the presence of Fourier flows and quadratic Boussinesq thermal oscillations. They ran the analysis for two different hybrid nanofluid formulations: Case-I and Case-II. Graphene (cylindrical), carbon nanotubes (spherical), and alumina (platelet) were considered for Case-I, while copper (cylindrical), copper oxide (spherical), and silver oxide (platelet) were studied in Case-II. In [22], it was shown that, in comparison to Case-II ternary combinations, the temperature distribution in Case-I ternary mixtures is greater. When compared to a mixture of copper (cylindrical), copper oxide (spherical), and silver (platelet), a mixture of graphene (cylindrical), carbon nanotubes (spherical), and aluminum oxide (platelet) has better conductivity. In addition, it was found that as the quadratic convection increased, the rate of heat transfer increased. Gupta and Rana [23] investigated the 3D magneto stagnation-point flow of ternary hybrid nanofluid induced by a radially extended infinitely rotating disk with multiple sliding effects. They conducted a comparative analysis of the heat transfer characteristics of linear thermal radiation, quadratic thermal radiation, and non-linear thermal radiation. As shown in [23], the heat transfer rate (Nusselt number) in the case of the nonlinear Rosseland approximation is higher than for the quadratic and linear approximations, and even higher for a ternary nanofluid compared to a pure liquid.

The abovementioned review of the literature revealed that no detailed studies have been done on the analysis of three different types of Rosseland thermal radiation on flow and heat transfer over a porous sheet that is stretching vertically under nonlinear (quadratic) convection. Thus, the novelty of this study was to conduct a comparative analysis of the mutual influence of three different forms of Rosseland thermal radiation and quadratic convection (quadratic density temperature variation) on a ternary nanofluid. So the aim of this study is to study the nonlinear convective flow and heat transfer of a ternary hybrid nanofluid in the boundary layer when a porous sheet is stretched under the action of an external transverse magnetic field. To our knowledge, such a study has not yet been described in the literature.

In the present study, we consider a ternary hybrid nanofluid formed by suspending three types of water-based CuO, Cu, and Ag nanoparticles. Mathematical formulation is carried out using the laws of conservation of mass, flow, and heat transfer. Joule heating and heat absorption/generation effects are included in the energy equations for three different forms of Rosseland thermal radiation. Basic partial differential equations are converted into a set of ordinary differential equations using a similarity transformation and then solved numerically using the *bvp* method in Maple software. The results obtained are presented graphically and discussed. In addition, the effects of skin friction and Nusselt numbers are described for three different forms of Rosseland thermal radiation.

2. Statement of the problem and mathematical model

Let us consider a two-dimensional convective flow of a ternary hybrid nanofluid on a porous stretching sheet in a gravity field (see Fig. 1). The x-axis is chosen to run parallel to the vertical surface, whereas the y-axis is chosen to run perpendicular to it. The surface velocity is assumed to be $u_w(x)$, and the applied magnetic field B_0 is determined along the sheet's normal. It is also assumed that the constant temperature of the sheet's surface is T_w, whereas the ambient fluid's is T_∞. The basic equations of ternary hybrid nanofluid for the flow can be defined as

$$\frac{\partial u}{\partial x} + \frac{\partial v}{\partial y} = 0 \tag{1}$$

$$u\frac{\partial u}{\partial x} + v\frac{\partial u}{\partial y} = \frac{\mu_{thf}}{\rho_{thf}}\frac{\partial^2 u}{\partial y^2} - \frac{\mu_{thf}}{K\rho_{thf}}u -$$

$$-\frac{\sigma_e}{\rho_{thf}}B_0^2 u + g\beta_0(T - T_\infty) + g\beta_1(T - T_\infty)^2 \tag{2}$$

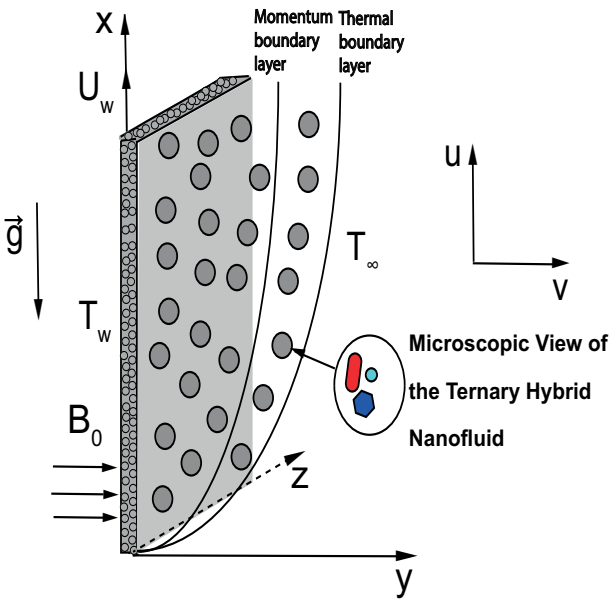

Fig. 1. The physical configuration and coordinate system of the problem.

$$u\frac{\partial T}{\partial x}+v\frac{\partial T}{\partial y}=\frac{k_{thf}}{(\rho C_p)_{thf}}\frac{\partial^2 T}{\partial y^2}-$$
$$-\frac{1}{(\rho C_p)_{thf}}\frac{\partial q_r}{\partial y}+\frac{Q_0\,(T-T_\infty)}{(\rho C_p)_{tnf}}+\frac{\sigma_e}{(\rho C_p)_{tnf}}B_0^2u^2 \tag{3}$$

All the terms involved in these equations are defined in nomenclature. The following are the boundary conditions for the investigated model:

$$u=U_w(x)=ax,\quad v=0,\quad T_w=T_\infty+bx^2,\quad \text{at}\quad y=0 \tag{4}$$

$$u\to 0,\quad v\to 0,\quad T=T_\infty,\quad \text{at}\quad y\to\infty \tag{5}$$

We assume that $U_w(x)=ax$ and $a>0$ for a stretching sheet. The physical quantities of interest are the local skin friction coefficient C_{fx}, the local Nusselt number Nu_x are defined as

$$C_{fx}=\frac{\mu_{thf}}{\rho_f a^2x^2}\left(\frac{\partial u}{\partial y}\right)_{y=0},$$
$$Nu_x=\frac{x}{k_f(T_w-T_\infty)}\left[-k_{thf}\left(\frac{\partial T}{\partial y}\right)_{y=0}+q_r|_{y=0}\right]. \tag{6}$$

Let the ternary hybrid nanofluid be composed of three sorts of nanoparticles, denoted by indices 1, 2, and 3. The spherical nanoparticles have a volume of 1, cylindrical nanoparticles have a volume of 2, and platelet nanoparticles have a volume of 3. The overall volume fraction is the sum of the volume concentrations of the three dissimilar kinds of nanoparticles:

$$\phi=\phi_1+\phi_2+\phi_3 \tag{7}$$

The viscosity and thermal conductivity of ternary nanofluid are as follows:

$$\frac{\mu_{tnf}}{\mu_f}=\frac{B_1\phi_1+B_2\phi_2+B_3\phi_3}{\phi},\ \frac{\kappa_{tnf}}{\kappa_f}=\frac{B_4\phi_1+B_5\phi_2+B_6\phi_3}{\phi}. \tag{8}$$

Next, the densities and heat capacities of a ternary hybrid nanofluid are

$$\frac{\rho_{tnf}}{\rho_f}=1-\phi_1-\phi_2-\phi_3+\phi_1\frac{\rho_{sp_1}}{\rho_{bf}}+\phi_2\frac{\rho_{sp_2}}{\rho_{bf}}+\phi_3\frac{\rho_{sp_3}}{\rho_{bf}},$$

$$\frac{(\rho C_p)_{tnf}}{(\rho C_p)_f} = 1 - \phi_1 - \phi_2 - \phi_3 + \phi_1 \frac{(\rho C_p)_{sp_1}}{(\rho C_p)_{bf}} + \phi_2 \frac{(\rho C_p)_{sp_2}}{(\rho C_p)_{bf}} + \phi_3 \frac{(\rho C_p)_{sp_3}}{(\rho C_p)_{bf}}. \tag{9}$$

In equation (8), coefficients B_1, B_4 correspond to spherical nanoparticles, B_2, B_5 – to cylindrical nanoparticles, B_3, B_6 – to platelet nanoparticles, and are defined as

$$B_1 = \frac{\mu_{nf_1}}{\mu_f} = 1 + 2.5\phi + 6.2\phi^2,$$

$$B_4 = \frac{\kappa_{nf_1}}{\kappa_f} = \frac{\kappa_{sp_1} + 2\kappa_f - 2\phi\left(\kappa_f - \kappa_{sp_1}\right)}{\kappa_{sp_1} + 2\kappa_f + \phi\left(\kappa_f - \kappa_{sp_1}\right)},$$

$$B_2 = \frac{\mu_{nf_2}}{\mu_f} = 1 + 13.5\phi + 904.4\phi^2,$$

$$B_5 = \frac{\kappa_{nf_2}}{\kappa_f} = \frac{\kappa_{sp_2} + 3.9\kappa_f - 3.9\phi\left(\kappa_f - \kappa_{sp_2}\right)}{\kappa_{sp_2} + 3.9\kappa_f + \phi\left(\kappa_f - \kappa_{sp_2}\right)},$$

$$B_3 = \frac{\mu_{nf_3}}{\mu_f} = 1 + 37.1\phi + 612.6\phi^2,$$

$$B_6 = \frac{\kappa_{nf_3}}{\kappa_f} = \frac{\kappa_{sp_3} + 4.7\kappa_f - 4.7\phi\left(\kappa_f - \kappa_{sp_3}\right)}{\kappa_{sp_3} + 4.7\kappa_f + \phi\left(\kappa_f - \kappa_{sp_3}\right)}. \tag{10}$$

Tab. 2 shows thermophysical constants for some sorts of nanoparticles and base fluids.

Property	H_2O	CuO	Cu	Ag
$\rho[kg \cdot m^{-3}]$	997.1	6500	8933	10500
$C_p[J \cdot kg^{-1} \cdot K^{-1}]$	4179	535.6	385	235
$k[W \cdot m^{-1} \cdot K^{-1}]$	0.613	20	400	429
Nanoparticle shapes	No	spherical	cylindrical	platelet

Numerical values of nanoparticles and base fluid characteristics.

3. Similarity transformation and physical quantities

The partial differential equations (1)-(3) are transformed into ordinary differential equations through similarity transformation:

$$u = axf'(\eta), \quad v = -\sqrt{a\nu_f} f(\eta), \quad \eta = y\sqrt{\frac{a}{\nu_f}}, \quad \theta(\eta) = \frac{T - T_\infty}{T_w - T_\infty}, \tag{11}$$

where f, θ are the dimensionless functions, η is the similarity variable. Primes denote differentiation with regard to η in this context. Note that streamlined flows in this study can be described by the stream function ψ, which is determined from the relations $u = \partial\psi/\partial y, v = -\partial\psi/\partial x$, satisfying the continuity equation (1). The radiative heat flux q_r can be defined as [6]

$$q_r = -\frac{4}{3k^*}\frac{\partial}{\partial y}(\sigma^* T^4) \tag{12}$$

The radiant heat flow q_r is given by using the Rosseland approximation for three cases:
1) Rosseland linear thermal radiation (RLTR)
Here we use Taylor series expansion to the term T^4 about T_∞ and ignoring the higher order terms

$$T^4 \cong 4T_\infty^3 T - 3T_\infty^4 \tag{13}$$

Eq. (13) is substituted into Eq. (12), and the resulting value is

$$q_r = -\frac{16\sigma^* T_\infty^3}{3k^*}\frac{\partial T}{\partial y}, \text{ and } -\frac{1}{(\rho C_p)_{thf}}\frac{\partial q_r}{\partial y} = \frac{16\sigma^* T_\infty^3}{3(\rho C_p)_{thf}k^*}\frac{\partial^2 T}{\partial y^2}. \tag{14}$$

2) Rosseland quadratic thermal radiation (RQTR)
Using the Taylor series expansion of T^4, we restrict ourselves to terms of the second order:

$$T^4 \approx T_\infty^4 + 4T_\infty^3(T - T_\infty) + 6T_\infty^2(T - T_\infty)^2 = 3T_\infty^4 - 8T_\infty^3 T + 6T_\infty^2 T^2 \tag{15}$$

Substituting Eq. (15) into Eq. (12), we get

$$q_r = \frac{32\sigma^* T_\infty^3}{3k^*}\frac{\partial T}{\partial y} - \frac{24\sigma^* T_\infty^2}{3k^*}\frac{\partial}{\partial y}T^2, \text{ and } -\frac{1}{(\rho C_p)_{thf}}\frac{\partial q_r}{\partial y} = -\frac{32\sigma^* T_\infty^3}{3(\rho C_p)_{thf}k^*}\frac{\partial^2 T}{\partial y^2} + \frac{24\sigma^* T_\infty^2}{3(\rho C_p)_{thf}k^*}\frac{\partial^2}{\partial y^2}T^2. \tag{16}$$

3) Rosseland nonlinear thermal radiation (RNTR)

$$-\frac{1}{(\rho C_p)_{thf}}\frac{\partial q_r}{\partial y} = \frac{16\sigma^*}{3(\rho C_p)_{thf}k^*}\left(3T^2\frac{\partial T}{\partial y}\frac{\partial T}{\partial y} + T^3\frac{\partial^2 T}{\partial y^2}\right). \tag{17}$$

On using (11), (14), (16), and (17), Eqs. (2)-(3) are transformed into the ordinary differential equations (ODEs) shown below:

$$A_1 f''' + ff'' - f'^2 - \epsilon_1 f' + \lambda\theta + \lambda Q_c\theta^2 = 0 \tag{18}$$

Energy equation with RLTR:

$$\epsilon_2\theta'' + f\theta' - 2f'\theta + A_2 Q\theta + A_2 M\mathrm{Ec}f'^2 = 0 \tag{19}$$

Energy equation with RQTR:

$$\epsilon_2\theta'' + \epsilon_3\theta\theta'' + f\theta' - 2f'\theta + \epsilon_3\theta'^2 + A_2 Q\theta + A_2 M\mathrm{Ec}f'^2 = 0 \tag{20}$$

Energy equation with RNTR:

$$\epsilon_2\theta'' + \epsilon_3\theta\theta'' + \epsilon_4\theta^2\theta'' + \epsilon_5\theta^3\theta'' + f\theta' - 2f'\theta + \epsilon_3\theta'^2 + \\ +2\epsilon_4\theta\theta'^2 + 3\epsilon_5\theta^2\theta'^2 + A_2 Q\theta + A_2 M\mathrm{Ec}f'^2 = 0 \tag{21}$$

In the above system of equations, the following ratios are used:

$$A_1 = \frac{\mu_{thf}/\mu_f}{\rho_{thf}/\rho_f},\ \epsilon_1 = A_1\widetilde{K} + \left(\frac{\rho_f}{\rho_{thf}}\right)M,\ \epsilon_2 = \frac{1}{Pr}\left(\frac{k_{thf}/k_f}{(\rho C_p)_{thf}/(\rho C_p)_f}\right) + A_2\left(\frac{Nr}{Pr}\right),\ A_2 = \frac{(\rho C_p)_f}{(\rho C_p)_{thf}},$$

$$\epsilon_3 = 3A_2\left(\frac{Nr}{Pr}\right)(\theta_p - 1),\ \epsilon_4 = 3A_2\left(\frac{Nr}{Pr}\right)(\theta_p - 1)^2,\ \epsilon_5 = A_2\left(\frac{Nr}{Pr}\right)(\theta_p - 1)^3. \tag{22}$$

Dimensionless numbers $\widetilde{K}, M, \lambda, Gr_x, Re_x, Pr, Nr, Q_c, Q, \theta_p$, and Ec denote the dimensionless permeability parameter, magnetic parameter, convection parameter, thermal Grashoff number, Reynolds number, Prandtl number, radiation parameter, parameter of the quadratic (nonlinear) Boussinesq approximation, heat absorption/generation, temperature ratio parameter, and Eckert number, respectively, where

$$\widetilde{K} = \frac{\nu_f}{aK},\ M = \frac{B_0^2\sigma_e}{a\rho_f},\ \lambda = \frac{Gr_x}{Re_x^2},\ Gr_x = \frac{g\beta_0(T_w - T_\infty)x^3}{\nu_f^2},\ Re_x = \frac{U_w x}{\nu_f},\ Pr = \frac{\nu_f(\rho C_p)_f}{k_f},$$

$$Nr = \frac{16\sigma^* T_\infty^3}{3k_f k^*},\ Q_c = \frac{\beta_1}{\beta_0}(T_w - T_\infty),\ Q = \frac{Q_0}{(\rho C_p)_f a},\ \theta_p = \frac{T_w}{T_\infty},\ \mathrm{Ec} = \frac{U_w^2}{(C_p)_f(T_w - T_\infty)}. \tag{23}$$

The related boundary conditions (4)-(5) are transformed as follows:

$$f(0) = 0, \quad f'(0) = 1, \quad \theta(0) = 1, \quad \text{at} \quad \eta = 0 \tag{24}$$

$$f'(\eta) \to 0, \quad f(\eta) \to 0, \quad \theta(\eta) \to 0, \quad \text{at} \quad \eta \to \infty \tag{25}$$

Next, using the similarity variables (11), one can easily obtain the expressions for physical quantities (6):

$$C_f = C_{fx}\sqrt{Re_x} = \frac{\mu_{thf}}{\mu_f} f''(0),$$

$$\text{for the RLTR approximation:} \quad Nu = Nu_x(\sqrt{Re_x})^{-1} = -\left(\frac{k_{thf}}{k_f} + Nr\right)\theta'(0),$$

$$\text{for the RQTR approximation:} \quad Nu = Nu_x(\sqrt{Re_x})^{-1} = -\left(\frac{k_{thf}}{k_f} + Nr + 3Nr\theta(0)(\theta_p - 1)\right)\theta'(0),$$

$$\text{for the RQTR approximation:} \quad Nu = Nu_x(\sqrt{Re_x})^{-1} = -\left(\frac{k_{thf}}{k_f} + Nr(1 + \theta(0)(\theta_p - 1))^3\right)\theta'(0). \tag{26}$$

4. Numerical method

In this study, a numerical analysis of the flow of a ternary hybrid nanofluid on a stretching porous sheet under the influence of a magnetic field, thermal absorption/generation, and thermal radiation is carried out. We have obtained equations (18)-(21), which are a system of strongly nonlinear ordinary differential equations for a ternary hybrid nanofluid in the linear, quadratic, and nonlinear Rosseland approximations. For numerical analysis, we use a water-based ternary hybrid nanofluid with the following composition: $CuO - Cu - Ag - H_2O$. Spherical copper oxide (CuO), cylindrical copper (Cu), and platelet silver (Ag) nanoparticles are examples of nanoparticle shapes (see Tab. 2). The *bvp* method in Maple computer software is used to solve dimensionless ordinary differential equations (18)-(21) with boundary conditions (24)-(25). In this method, suitable finite values of η_∞ that are replaced by η_{10} must be chosen. As a result, all calculations were performed for $\eta_\infty = 10$ for boundary conditions (25) with an accuracy of 10^{-5} .

5. Results and discussion

This section graphically presents the numerical results of the influence of the parameters of the magnetic field M, thermal radiation Nr, mixed convection λ, the nonlinear Boussinesq approximation Q_c, Eckert number Ec, and the volume concentration of the nanofluid ϕ on dimensionless profiles of velocity $f'(\eta)$ and temperature $\theta(\eta)$, the skin friction coefficient (C_f), as well as the Nusselt number (Nu), for different Rosseland approximations. When performing numerical calculations, we assume that the volume concentration of nanoparticles and the Prandtl number are $\phi = 0.06$ and $Pr = 4$, respectively. Ternary hybrid nanofluids are studied for 1% of spherical copper oxide (CuO), 2% of cylindrical copper (Cu), and 3% of platelet-sized silver (Ag) nanoparticles. The calculations are done for $M = 0.5, \widetilde{K} = 1/9, \lambda = 0.3, Nr = 1, Q_c = 0.1, Q = 0.1, \theta_p = 2.5$ and $Ec = 0.5$.

51 Velocity and thermal characteristics

At a fixed value of other parameters, Figures 2a and 2b depict the effect of the magnetic field on the velocity profile and temperature profile of the ternary hybrid nanofluid, respectively. An external magnetic field generates a force called the Lorentz force, which opposes the flow of the fluid. The magnitude of this force is directly proportional to the magnitude of M. Therefore, an increase in M enhances the Lorentz force. As M values increase, the velocity profile decreases due to increased resistance to fluid flow. Slowing down the flow rate allows the nanoparticles

to conduct more heat, and hence a temperature rise occurs. This is especially noticeable for RNTR compared to other cases (RLTR, RQTR).

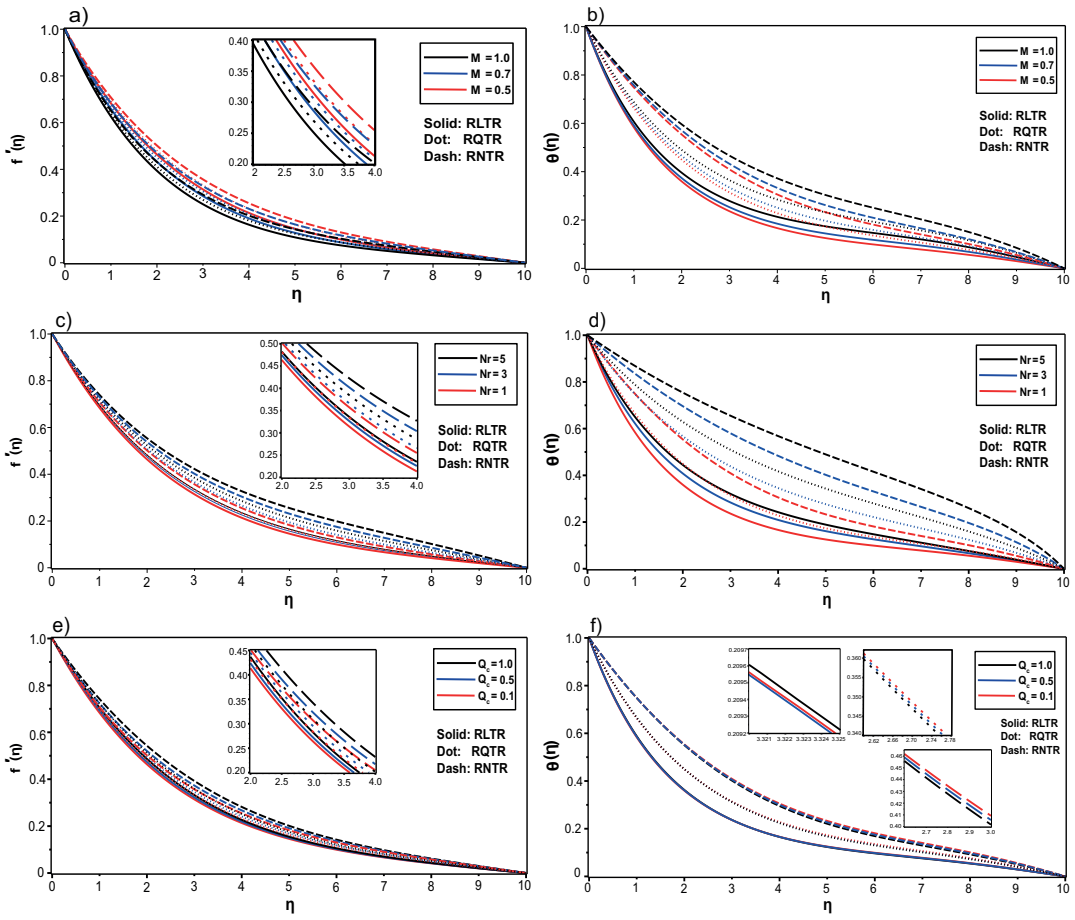

Fig. 2. (a)-(b) Effect of M on $f'(\eta)$ and $\theta(\eta)$; (c)-(d) velocity and temperature profiles for various Nr values; (e)-(f) velocity and temperature profiles for various Q_c values. Graphs are built for RLTR, RQTR, and RNTR cases.

Figures 2c and 2d show the influence of the radiation parameter Nr on the velocity $f'(\eta)$ and temperature $\theta(\eta)$ profiles for various cases of the Rosseland approximation. An increase in the Nr parameter leads to an increase in the flow velocity since an additional part of the radiative heat is transformed into the kinetic energy of the nanofluid flow. The temperature profile also increases as a result of an increase in thermal radiation. This effect is significant at large temperature gradients, when it is necessary to apply the quadratic or nonlinear Rosseland approximation.

The effect of the influence of the quadratic (nonlinear) parameter Boussinesq approximation Q_c on velocity and temperature profiles is presented in Figures 2e and 2f. Since the increase in the parameter Q_c is associated with an increase in the temperature difference, we observe an increase in temperature in the quadratic and nonlinear Rosseland approximations that is higher than in the linear one. As can be seen from Fig. 2e, the increase in parameter Q_c has a less noticeable effect on the velocity profile than on the temperature profile.

Figures 3a and 3b show how the convective parameter λ affects the velocity and temperature profiles for the RLTR, RQTR, and RNTR cases. An increase in the convection parameter λ is directly related to the dominant influence of buoyancy forces, which naturally leads to a restructuring of the flow and, as a consequence, an increase in the velocity profile in all cases of the Rosseland approximation. As can be seen from Fig. 3b, an increase in the convective parameter λ has a twofold effect on the temperature profile, i.e., near the boundary of the surface, the temperature increases with an increase in λ and decreases far away.

The effect of the heat generation/adsorption parameter Q and the Eckart number Ec on the velocity

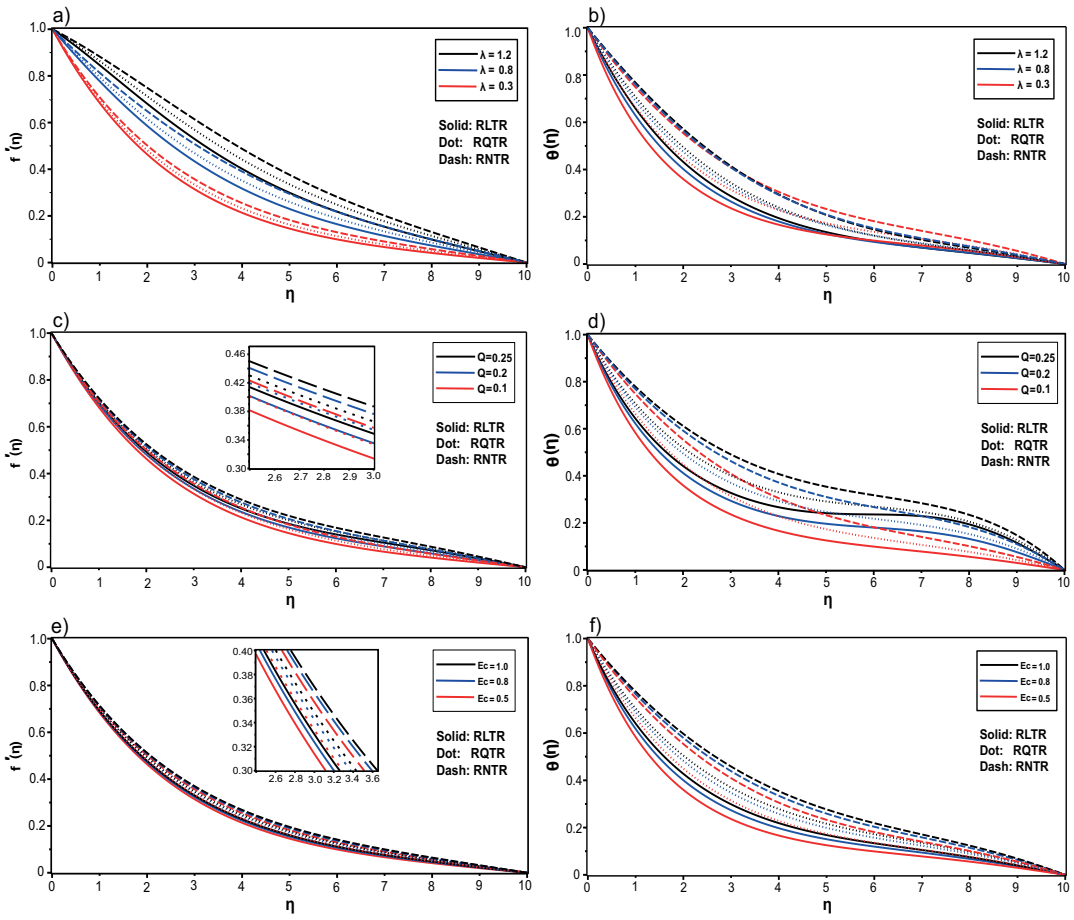

Fig. 3. (a)-(b) Impact of λ on $f'(\eta)$ and $\theta(\eta)$; (c)-(d) impact of Q on $f'(\eta)$ and $\theta(\eta)$; (e)-(f) impact of Ec on $f'(\eta)$ and $\theta(\eta)$. Graphs are built for the RLTR, RQTR and RNTR cases.

and temperature profiles is shown in Figures 3c-3d and 3e-3f. Hence, we see that in all cases of the Rosseland approximation, an increase in the parameters Q and Ec increases the temperature of the hybrid nanofluid.

The Eckart number shows the relationship between kinetic energy and the change in thermal enthalpy. It is obvious that as Ec rises, the hybrid nanofluid's kinetic energy rises as well, increasing the velocity profile.

The velocities and temperature profiles of the hybrid nanofluid increase as the volume fraction of silver nanoparticles ϕ_3 increases in all cases of the Rosseland approximation, as shown in Figures 4a and 4b. The improvement in the temperature profile is associated with an increase in the thermal conductivity of the hybrid nanofluid when silver nanoparticles ϕ_3 are added to the base fluid. This suggests that the appliance's ability to absorb heat is improved, ensuring an ideal temperature and a long life for the device. We also observe an increase in temperature in the quadratic and nonlinear Rosseland approximations that is higher than in the linear one. The fluid flow rate increases, as shown in Fig. 4a, due to the increase in kinetic energy at the increased temperature (thermal energy).

52 Skin friction and Nusselt number

In this section, plots of the behavior of the friction coefficient S_f and Nusselt number Nu on some dimensionless parameters are given for various cases of the Rosseland approximation.

As can be seen from Fig. 5a, with an increase in the parameter M, the skin friction coefficient S_f decreases. This is due to the fact that with an increase in M, the Lorentz force increases, which leads to

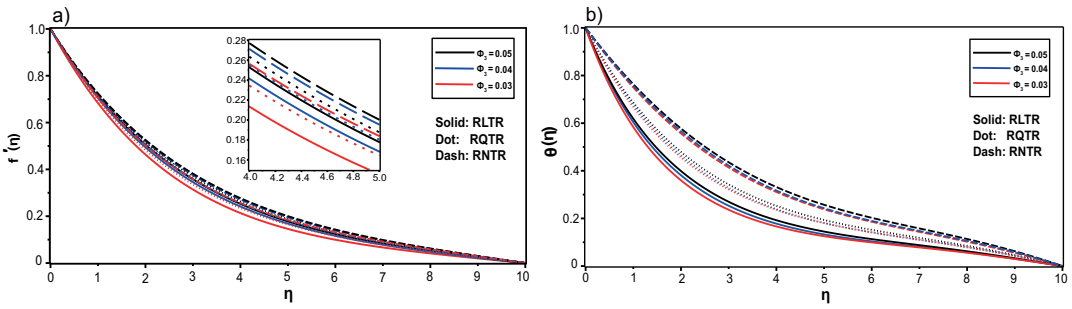

Fig. 4. Impact of ϕ_3 on $f'(\eta)$ and $\theta(\eta)$ for the RLTR, RQTR and RNTR cases.

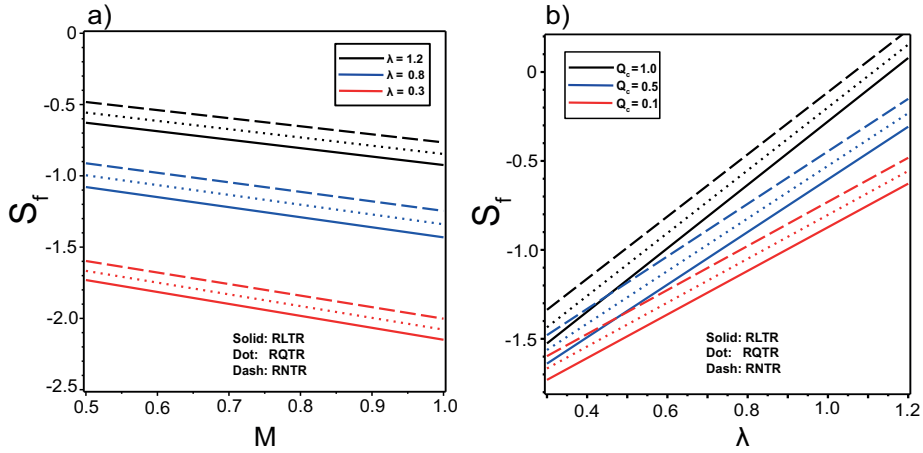

Fig. 5. a) The influence of the convection parameter λ and magnetic field M on the skin friction coefficient S_f; b) the effect of the nonlinear Boussinesq Q_c and convection λ parameters on the skin friction coefficient S_f.

deceleration of the nanofluid flow and, as a consequence, a decrease in the value of C_f. The skin friction coefficient on the other hand, increases when the convection parameter λ increases. This happens as a result of the flow velocity increasing with an increase in the parameter λ (see Fig. 3a), which in response causes an increase in the skin friction coefficient. This effect is especially noticeable for the cases of the quadratic and nonlinear Rosseland approximations as compared to the linear one.

Figure 5b shows that as the parameter of the quadratic (nonlinear) Boussinesq approximation increases, the skin friction coefficient increases as a result of an improvement in the velocity profile (see Fig. 2e). This effect is also especially noticeable in the cases of the quadratic and nonlinear Rosseland approximations as compared to the linear one.

Figures 6a-6b and 6c-6d display the impact of the radiation parameter Nr and the Prandtl number Pr on the rate of heat transfer depending on the growth of the magnetic field parameter M for the cases of linear, quadratic, and nonlinear Rosseland approximations. These graphs show that Nu decreases as the parameter M increases. On the contrary, an increase in the parameters Nr and Pr leads to an increase in Nu. Figures 6a-6b and 6c-6d demonstrate that the nonlinear Rosseland approximation has a larger heat transfer rate than the quadratic and linear cases. This is completely justified because the rate of heat transfer is higher at large temperature gradients, when the nonlinear Rosseland approximation is appropriate.

As shown in Fig. 6e-6f, with an increase in the convection parameter λ against the background of an increase in parameters Q and Ec, the heat transfer rate decreases. On Fig. 6e-6f, it is also shown that the nonlinear Rosseland approximation has a higher heat transfer rate than the quadratic and linear cases.

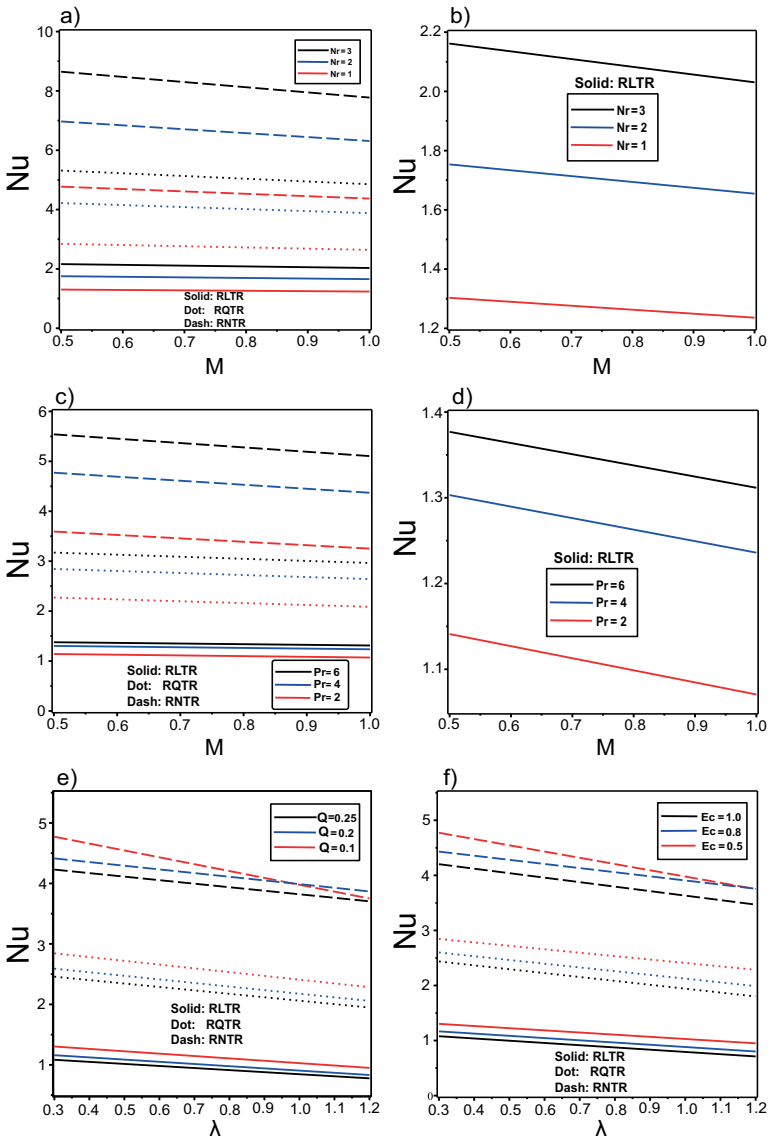

Fig. 6. a) The effect of the radiation parameter Nr and magnetic field M on the Nusselt number Nu; b) for the case of RLTR, a more detailed graph of the influence of the radiation parameter Nr and the magnetic field M on the Nusselt number Nu; c) the effect of Prandtl number Pr and magnetic field M on the Nusselt number Nu; d) for the case of RLTR, a more detailed graph of the influence of Prandtl number Pr and the magnetic field M on the Nusselt number Nu; e) the influence of the convection λ and heat absorption/generation Q parameters on the Nusselt number Nu; f) the effect of the convection λ parameter and Eckert number Ec on the Nusselt number Nu.

6. Conclusion

In this study, we have investigated the MHD flow of a ternary hybrid nanofluid past a linearly stretching vertical porous sheet, taking into account the effects of the Bousinesq quadratic approximation and three different forms of the Rosseland approximation: linear, quadratic, and nonlinear radiation effects. In our analysis, we used the thermophysical properties of a ternary hybrid nanofluid CuO-Cu-Ag-H_2O with nanoparticles of various densities and shapes. The *bvp* method in the Maple software was used to solve the self-similarity governing equations. The main results of this study are as follows:

1. Increasing the parameters radiation Nr, the quadratic Boussinesq approximation Q_c, convection λ, heat absorption/generation Q, Eckert number Ec, and the volume fraction of silver nanoparticles

ϕ_3 leads to an increase in the nanofluid flow rate. In this case, the velocity profiles and the thickness of the boundary layer are smaller for case RLTR compared to cases RQTR and RNTR.

2. The ternary hybrid nanofluid flow rate is decreased by the growing magnetic field M.
3. An increase in the magnetic field M leads to an increase in the temperature of the nanofluid, much more so in case RNTR than in cases RLTR and RQTR.
4. The absolute value of skin friction coefficients C_f increases with an increase in the magnetic field parameter M and decreases with an increase in the convection parameter λ and the quadratic Boussinesq approximation Q_c parameter. In this case, the absolute value of skin friction coefficients C_f is smaller for case RNTR than for cases RQTR and RLTR.
5. The local Nusselt number (rate of heat transfer) Nu decreases as the values of the parameters Pr, Nr, and M increase. On the other hand, an increase in the value of parameters Q and Ec reduces the heat transfer rate Nu with an increase in parameter λ.

This paper investigated some flow and heat transfer phenomena along an stretching porous vertical plate. The phenomena of convective heat transfer with thermal radiation are observed in solar power plants, gas production, spacecraft, etc. Therefore, the present study can find application in the systems listed above. However, our attention was limited to the two-dimensional flow of a Newtonian ternary hybrid nanofluid, taking into account the quadratic Boussinesq approximation and three different forms of Rossland thermal radiation. Therefore, in future studies, three-dimensional flows of non-Newtonian nanofluids along an stretching/shrinking surface in two lateral directions can be considered, taking into account the influence of external forces, such as the Lorentz and Coriolis forces.

References

1. S. L. Goren, *Chem. Eng. Sci.*, **6-7**, 515 (1966)
2. K. Vajravelu, K. S. Sastri, *Int. J. Heat Mass Transf.*, **20**, 655 (1977).
3. M. K. Partha, *Appl. Math. Mech.*, **31**, 565 (2010).
4. C. RamReddy, P. Naveen, D. Srinivasacharya, *Nonlinear Engineering*, **8**, 94 (2019).
5. S.U.S. Choi, J. A. Eastman, *Am. Soc. Mech. Eng. Fluids Eng. Div. FED.*, **231**, 99 (1995).
6. S. Rosseland, *Astrophysik aud Atom-Theoretische Grundlagen* (Springer: Berlin/Heidelberg, Germany), 1931.
7. Viskanta R., Grosh R.J. *Int. J. Heat Mass Transf.* **1962**, 5, 795-806.
8. C. Perdikis, A. Raptis, *Heat Mass Transf.*, **31**, 381 (1996).
9. R. Cortell, *Chin. Phys. Lett.*, **25**, 1340 (2008).
10. A. Pantokratoras, *Int. J. Therm. Sci.*, **84**, 151 (2014).
11. B. K. Jha, G. Samaila, *JPME*, 236 (2021).
12. M. Waqas, S. A. Shehzad, T. Hayat, M. I. Khan, A. Alsaedi, *J. Phys. Chem. Solids*, **133**, 45 (2019).
13. B. Mahanthesh, *Quadratic Radiation and Quadratic Boussinesq Approximation on Hybrid Nanoliquid Flow.* In Mathematical Fluid Mechanics, De Gruyter Berlin, Germany, 2021, pp. 13-54.
14. K. Thriveni, B. Mahanthesh, Int. Commun. Heat Mass Transf., **124**, 105264 (2021).
15. B. Mahanthesh, T. V. Joseph, K. Thriveni, *Dynamics of non-Newtonian nanoliquid with quadratic thermal convection.* Mathematical Fluid Mechanics: Advances in Convective Instabilities and Incompressible Fluid Flow, edited by B. Mahanthesh, Berlin, Boston: De Gruyter, 2021, pp. 223-248.
16. T. Anusha, U.S. Mahabaleshwar, Y. Sheikhnejad, *Transp. Porous Med.*, **142**, 333 (2021).
17. G. K. Ramesh, J.K. Madhukesh, S.A. Shehzad, A. Rauf, *Proc. Inst. Mech. Eng. E: J. Process Mech. Eng.*, **2022**, 1-10 (2022).
18. S. Manjunatha, V. Puneeth, B. J. Gireesha, A. J. Chamkha, *J. Appl. Comput. Mech.*,**8**, 1279 (2022).
19. I. L. Animasaun, S. J. Yook, T. Muhammad, A. Mathew, *Surf. Interfaces*, **28**, 101654 (2022).
20. T. Maranna, U. S. Mahabaleshwar, M. I. Kopp, *J. App. Comp. Mech.*, online from 24 October 2022 (2023) (in print).
21. K. Guedri et al., *Mathematical Problems in Engineering*, Volume 2022, Article ID 3429439, 14 pages (2022).
22. K. Sajjan et al., *AIMS Mathematics*, **7**, 18416 (2022).
23. G. Gupta, P. Rana, *Mathematics*, **10**, 3342 (2022).